# Resolving the dynamic structure of chlorosomes in green sulfur bacteria by MAS NMR

Dsouza, L.A.

# Chapter 1

# Introduction and Methodological background

# A General Introduction

## 1.1 Introduction

Fossil fuels are currently one of the most widely used energy sources, but they will eventually become depleted in the future, leading to an energy crisis. Additionally, the use of fossil fuels is not an ideal solution due to their negative impacts on society and the environment, including global warming, air pollution, and political tensions, as they are not evenly distributed worldwide.[1,2]

There are many renewable energy sources the planet has to offer to humankind, and among them, solar energy is the largest. The utilization of solar energy for power generation through methods such as photovoltaic cells is a prevalent practice. Despite this, the full potential of this energy source remains inadequately realized. The solution to this problem can be found by going back to nature, where the energy from the sun is utilized efficiently by a process called photosynthesis, a fundamental mechanism that supports and sustains most life on Earth. There has been growing research towards mimicking natural photosynthesis and using it in artificial photosynthesis to harness solar energy efficiently.[1,3–5]

Photosynthesis is a complex, multi-step process that begins with the capture of light energy, followed by its transfer to the reaction center, where charge separation occurs.[6,7] The harvesting of light is crucial as it is the first step in photosynthesis, and it is carried out by antennae in photosynthetic organisms. A wide variety of light-harvesting antennae consisting of various pigments such as chlorophylls, bacteriochlorophylls, phycobilins, carotenoids, etc., are known to exist.[8,9] The interaction of pigments with their environment dictates their properties. The dynamics occurring on the molecular and cellular level are related to their environment, which in turn governs their functionality.[10,11] The chlorosomes of green sulfur bacteria are recognized as the largest light-harvesting antennae observed in nature. Chlorosomes are considered robust because of the presence of a dense assembly of self-aggregated bacteriochlorophyll molecules and the arrangement of these pigments in a way that drives efficient exciton energy transfer upon photon absorption.[8] The self-aggregation of pigments without encoding the proteins makes them a preferred candidate for mimicking artificial photosynthesis.[12–18]

## 1.2 Photosynthetic Bacteria

Photosynthetic bacteria are broadly categorized into two groups based on the type of photosynthesis they perform: oxygenic and anoxygenic. In oxygenic photosynthesis, water serves as the electron donor, and molecular oxygen is released as a by-product. This mode of photosynthesis is carried out by plants as well as by cyanobacteria, which include several subclasses such as prochlorophytes. In contrast, anoxygenic photosynthesis employs alternative electron donors such as hydrogen sulfide or organic compounds. When hydrogen sulfide is utilized, the organisms are classified as green or purple sulfur bacteria, whereas the use of organic substrates as electron donors characterizes green and purple non-sulfur bacteria (Figure 1.1).[19–21] I will concentrate on green bacteria and in particular green sulfur bacteria in this thesis.

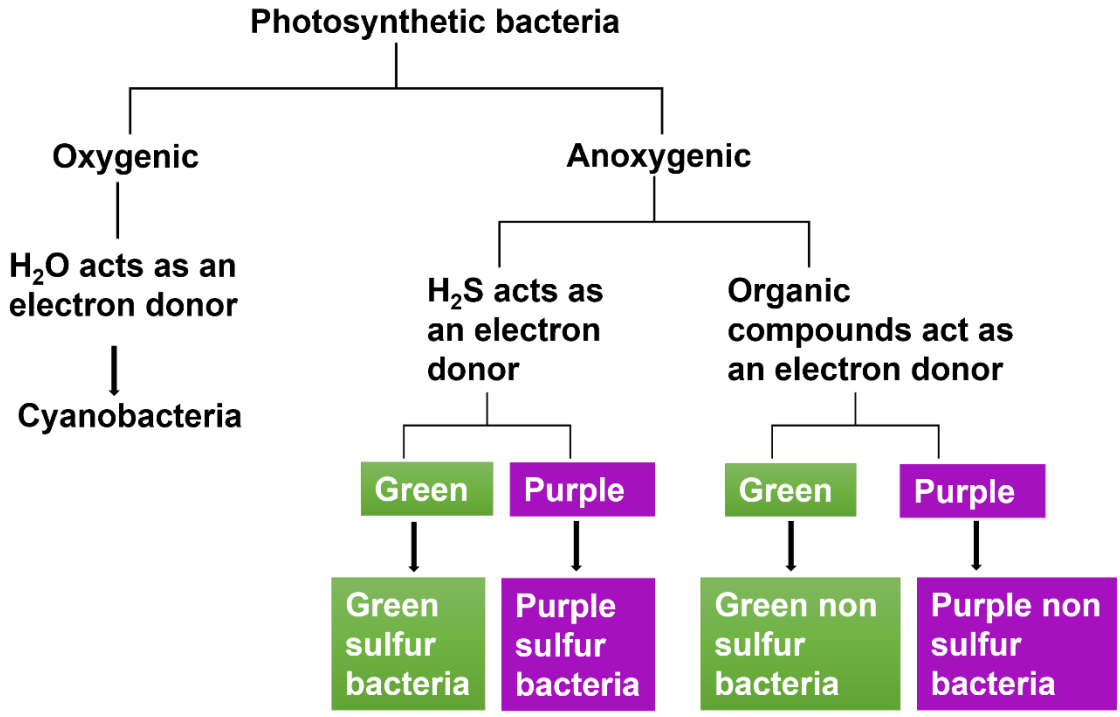


**Figure 1.1** Classification of photosynthetic bacteria.

## 1.3 Green Bacteria

Green bacteria are a group of anoxygenic bacteria characterized by their unique light-harvesting structures known as chlorosomes. These bacteria belong to three distinct phyla:

*Chlorobi*, *Candidatus Chloroacidobacterium thermophilum*, and filamentous anoxygenic phototrophs of the phylum *Chloroflexi.* All three have special antennae systems, chlorosomes, as the light-harvesting apparatus. Despite their diversity, green bacteria thus share the common feature of chlorosomes, which serve as specialized antennae systems for capturing light energy.[22,23] Among these groups, *Chlorobaculum tepidum*, a species of green sulfur bacteria, is the most extensively studied and has emerged as a model organism for chlorosome research.[24] Green sulfur bacteria are predominantly found in environments such as hot springs and the deep waters of the Black Sea, where light intensity is extremely limited. At these depths, the environment is also devoid of oxygen, making it an ideal habitat for these anoxygenic phototrophs.[22,25–29]In this thesis, I focus on studying the structure and dynamics of chlorosomes due to their exceptionally efficient energy transfer capabilities, which are crucial for the survival of green bacteria in such harsh environments. Without this high efficiency, these organisms would not be able to thrive under the challenging conditions of low light and oxygen scarcity.[24]

## 1.4 The Introduction to Chlorosomes

The chlorosomes of green bacteria contain tubular molecular aggregates of BChl and are located on the inner side of the lipid envelope, interspersed with proteins. On average, chlorosomes are 50-60 nm in diameter and 120-150 nm in length.[24,30,31] Chlorosomes contain excitonically coupled pigments, and green bacteria contain either BChl *c*, *d*, or *e* pigments in them, along with a small amount of carotenoids and other pigments.[32] Each cell of *Cba. tepidum* contains *ca* 200 chlorosomes, and each chlorosome can contain 250,000 bacteriochlorophyll pigments, leading to *ca* 50 million bacteriochlorophylls per cell. In addition, they also contain minor amounts of carotenoids, quinones, and lipids. The lipid envelope consists of glycolipids, wax esters, and phospholipids along with a few proteins. On one side of the envelope, it is thought to have a para-crystalline two-dimensional baseplate made of CsmA-BChl *a*.[33–36] This baseplate connects to the FMO antenna complex and the reaction centre [37,38] Green sulfur bacteria also use a photosynthetic reaction centre where charge separation takes place.[39]

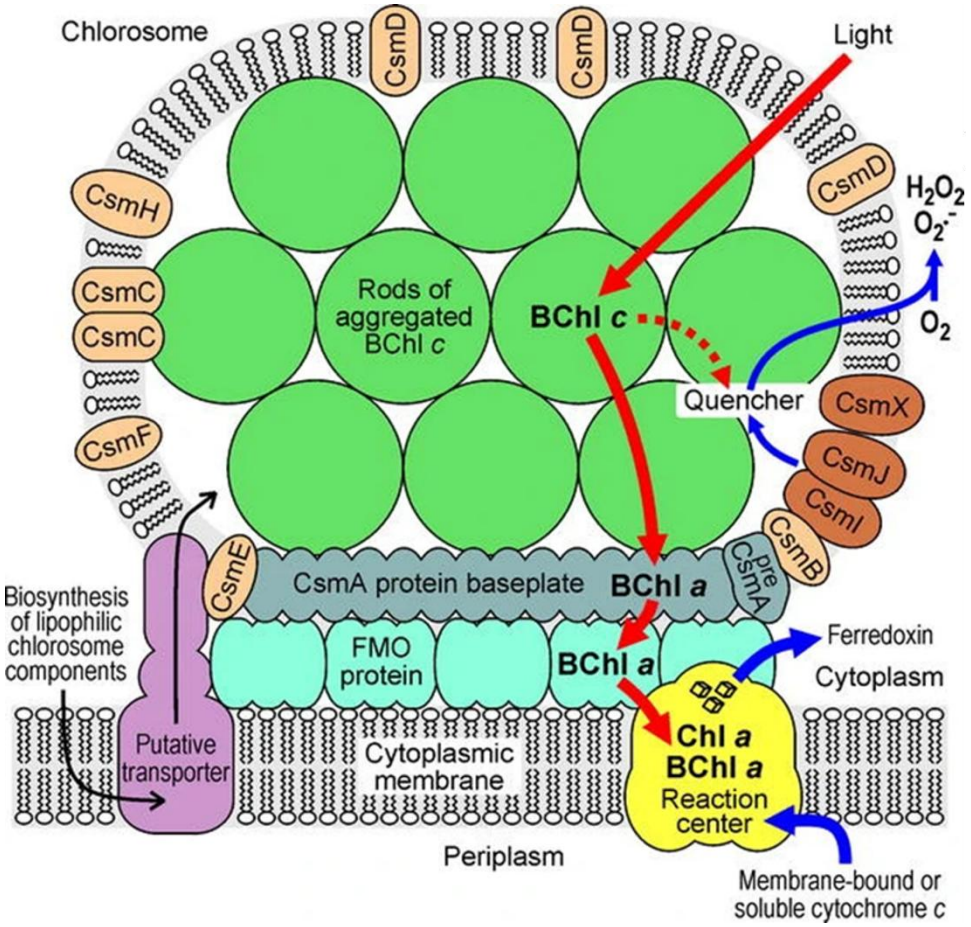


**Figure 1.2** Photosynthetic apparatus of *Cba. tepidum* (schematic). Picture reproduced with permission from Springer Nature.[36]

# Experimental and Methodological Insights into Solid-State NMR

## 1.5 General Introduction to Solid-State NMR

Solid-state NMR is a technique that is used in studying the structure and dynamics at an atomistic level of resolution. To understand this technique, it is necessary to dive into various interactions originating in NMR.

The spin Hamiltonian, which describes various interactions in solid-state NMR is given by the equation

$H = H_0 + H_{CS} + H_D + H_J + \ldots$

(1)

The external static field is given by $\mathbf{B}_0 = B_0 \mathbf{e}_z$

(2)

When a sample is placed in an external static magnetic field $\mathbf{B}_0$ the spins associated with the sample interact with the magnetic field and this is termed as Zeeman interaction and is given by

$$H_0 = -\boldsymbol{\mu} \cdot \mathbf{B}_0, \quad (3)$$

where $\boldsymbol{\mu}$ is the nuclear magnetic moment. $\boldsymbol{\mu}$ can be expressed in terms of the nuclear spin operator $\mathbf{I}$ as $\boldsymbol{\mu} = \gamma\hbar\mathbf{I}$. Equation 3 can be rewritten in units of $\hbar$ as

$$H_0 = -\gamma I_z B_0. \quad (4)$$

The Zeeman interaction is the dominant interaction in NMR since the strength of this interaction is in the order of $10^7$-$10^9$ Hz. However, the Zeeman interaction does not give any spectral information.[40] The field felt by the nucleus locally is not only due to the external magnetic field strength $B_0$ but also the field strength that is created locally ($B_{\text{loc}}$) by circulating electrons in the electron cloud around the nucleus that shields the nucleus from the $B_0$. The effective field felt by the nucleus is $B_{\text{eff}} = B_0 - B_{\text{loc}}$, and this results in a change in the resonance frequency of a nucleus. This interaction of spins with the local magnetic field is called the chemical shift interaction. The chemical shielding Hamiltonian on spin $I$ is given by

$$H_{\text{CS}} = -\gamma \mathbf{I}.\boldsymbol{\sigma}.\mathbf{B}_0, \quad (5)$$

where γ is the gyromagnetic ratio, and $\boldsymbol{\sigma}$ is the chemical shielding tensor whose value depends on the orientation of a molecule with respect to the magnetic field $\mathbf{B_0}$.

The electronic distribution around a nucleus is not always spherically symmetric as it depends on the orientation of the molecule in the magnetic field $\mathbf{B}_0$. The chemical shielding tensor is represented by a 3×3 matrix, which describes the orientation dependence of the chemical shift or chemical shielding anisotropy (CSA). A detailed explanation of CSA can be found, *e.g.* in[41].

The ensemble of spins, whether consisting of I spins or S spins, can interact with nuclei of the same type or different types. However, these interactions are significantly weaker than Zeeman interactions by several orders of magnitude. These interactions can be intramolecular or intermolecular. The interactions between two spins can be either through space or through a covalent bond between the spins. The through-space interactions are most often dipolar couplings, and the dipolar coupling Hamiltonian is given by

$$H_{\text{D}} = H_{\text{D}}^{II} + H_{\text{D}}^{IS} \quad (6)$$

where $H_{\mathrm{D}}^{II}$ is coined to describe the coupling between the same type of spins and is often referred to as homonuclear dipolar couplings, while $H_{\mathrm{D}}^{IS}$ is used to describe the coupling between two different spin types or heteronuclear dipolar couplings.

The Hamiltonians describing the homonuclear and heteronuclear dipolar couplings are given by

$$H_{\mathrm{D}}^{II} = -\frac{\mu^0}{4\pi}\hbar\sum_i\sum_j \frac{\gamma^I\gamma^I}{r_{ij}^3}\frac{1}{2}\left(3\cos^2\theta_{ij}-1\right)\left(3I_z^i-\mathbf{I}^i\cdot\mathbf{I}^j\right) \quad (7)$$

and

$$H_{\mathrm{D}}^{IS} = -\frac{\mu^0}{4\pi}\hbar\sum_i\sum_j \frac{\gamma^I\gamma^S}{r_{ij}^3}\frac{1}{2}\left(3\cos^2\theta_{ij}-1\right)2I_z^i S_z^j \quad (8)$$

where $r_{ij}$ represents the internuclear distance between two interacting spins, $\gamma^I$ and $\gamma^S$ are the gyromagnetic ratios of spins *I* and *S,* respectively, $\mu_o$ is the permeability of vacuum, $\theta_{ij}$ represents the angle between the internuclear vector **r** and the external magnetic field $\mathbf{B}_0$, and $I_z^i$ and $S_z^j$ are the z components of the nuclear spin angular momentum.

Measurement of dipolar couplings gives direct evidence for specific distances between two nuclei, which in turn helps in structure elucidation unambiguously.[42]

*J*-couplings offer direct insight into chemical bonding. Also referred to as scalar couplings, these field-independent interactions typically fall within the range of 1–$10^3$ Hz.Two spins can have a measurable *J* coupling if they are separated by very few bonds. Unlike dipolar couplings, these interactions are exclusively intramolecular. Even though their interaction is a few orders of magnitude lower than that of the dipolar couplings, mobile sites can be probed by the measurement of scalar-based experiments in solids.[43]

The Hamiltonian for scalar couplings is given by

$$H_{\mathrm{J}} = 2\pi J_{jk}(\mathbf{I}^j\cdot\mathbf{I}^k) \quad (9)$$

Here, $J_{jk}$ denotes the isotropic J-coupling.

## 1.6 Magic Angle Spinning NMR.

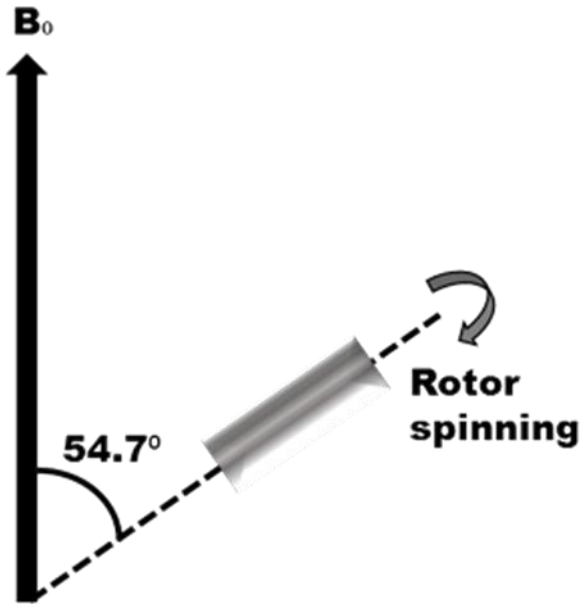


**Figure 1.3** schematics of spinning a sample at the magic angle of 54.7º with respect to the static magnetic field $\mathbf{B}_0$.

Magic angle spinning is a widely used technique in solids to remove the anisotropic interactions that arise due to the orientational dependency of the molecules with respect to chemical shielding tensors, and often they are referred to as chemical shift anisotropy. Contrary to solids, liquids have a rapid tumbling motion of the molecules, which averages the orientational dependency and gives rise to sharp, well-resolved lines in the spectra. To overcome the powder pattern seen in the solid-state NMR spectra, there was a need to develop a technique, and this is referred to as Magic Angle Spinning (MAS).[44,45] MAS is a technique that makes use of spinning a sample at the magic angle of 54.7º with respect to the external field $\mathbf{B}_0$, during which the anisotropic interactions, such as CSA and heteronuclear couplings, are scaled by the factor of $3\cos^2\theta$-1, become time-dependent, and can be averaged to zero at very high spinning frequencies.[46] When the MAS rotation exceeds the strong dipolar couplings, homonuclear couplings are also attenuated or removed. In MAS, averaging is given by

$$3\cos^2\theta_m-1=0, \qquad (10)$$

where $\theta_m$ = 54.7º is the magic angle.

MAS makes the inhomogenously broadened lines into narrower central lines with spinning side bands spaced at equal distances from the central band displaced by multiples of the spinning frequency used.

## 1.7 Dynamic Spectral Editing (DYSE) Technique in Solid-State NMR

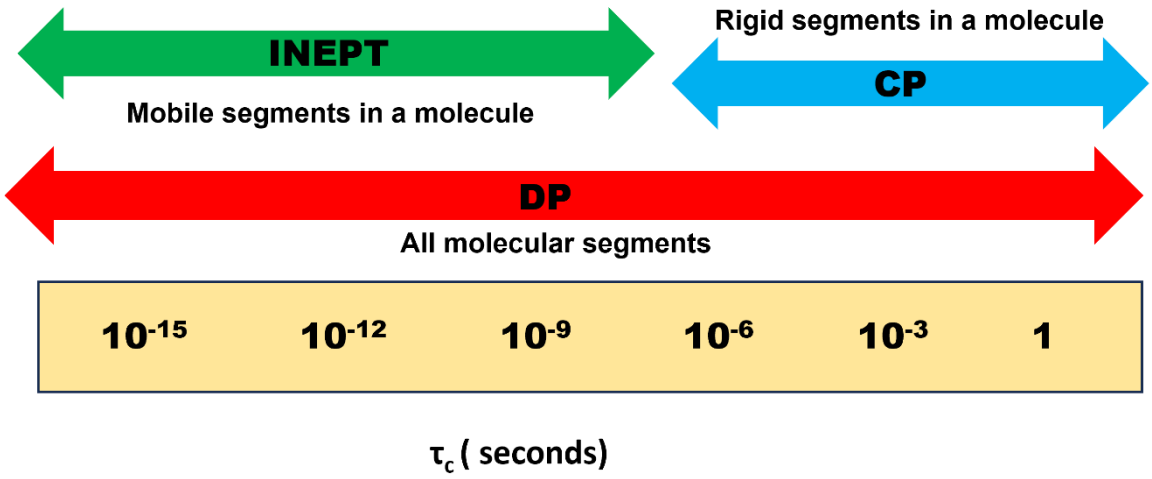


**Figure 1.4** Schematic representation of DP, CP and INEPT where the respective techniques are most effective.

Dynamic spectral editing is a technique where polarization transfer methods are employed to probe rigid and dynamic parts of the system under study. The transfer takes place from the spins with a high gyromagnetic ratio (γ) such as $^{1}H$ to the spins of a lower gyromagnetic ratio such as $^{13}C$ to enhance the signal intensity. The polarization transfer can be either through space or through a bond and this transfer acts as a dynamic filter. Through space transfer probes dipolar couplings between nuclei and through bond transfer probes *J*-couplings between nuclei. Through space transfer is done via cross polarization (CP) and through bond transfer is done via 'Insensitive Nuclei Enhanced Polarization Transfer' (INEPT).[47] It is interesting to know how these two act as dynamic filters. CP measures rigid molecular sites in a molecule. When there is large amplitude motion, the dipolar couplings are attenuated by averaging, making CP inefficient and as a result, the mobile sites are filtered out from the CP-based spectra that selectively show the NMR response from immobile constituents. On the other hand, if the coherence lifetime ($T_2$) is sufficiently long compared to the transfer time then INEPT becomes effective. This is not the case for rigid solids and hence INEPT acts as a

dynamic filter for selectively probing mobile constituents. Through bond transfer is also not affected by bond reorientation and as a result, they can be probed via INEPT type measurements. To combine the output of both filters, we used Direct Polarization (DP) which is not very sensitive to rigidity or flexibility within the molecule and provides insight into the NMR response irrespective of the dynamics. [43,48–51]

**Direct Polarization**

This simple technique begins with the application of a 90º pulse directly on the $^{13}C$ and applying a decoupling pulse on the protons while detecting the carbons. This particular sequence is not commonly used due to the fact that the abundance of $^{13}C$ in nature is quite low at just 1%. Therefore, labeling strategies need to be implemented to obtain accurate results. Even after the sample is fully labeled, the long $T_1$ of $^{13}C$ presents a challenge as the delay required to acquire the full signal must be sufficiently long. This results in a longer time needed to acquire the spectra compared to CP spectra. As a solution, CP or INEPT sequences are typically used for obtaining $^{13}C$ spectra.

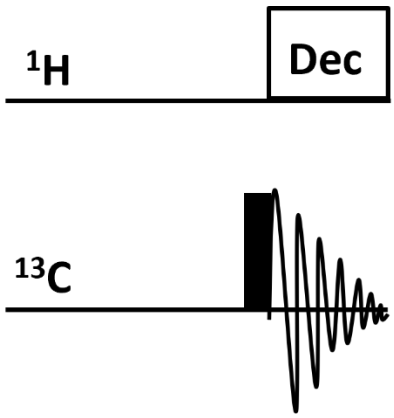


**Figure 1.5** Pulse sequence for Direct Polarization (DP)

**Cross Polarization**

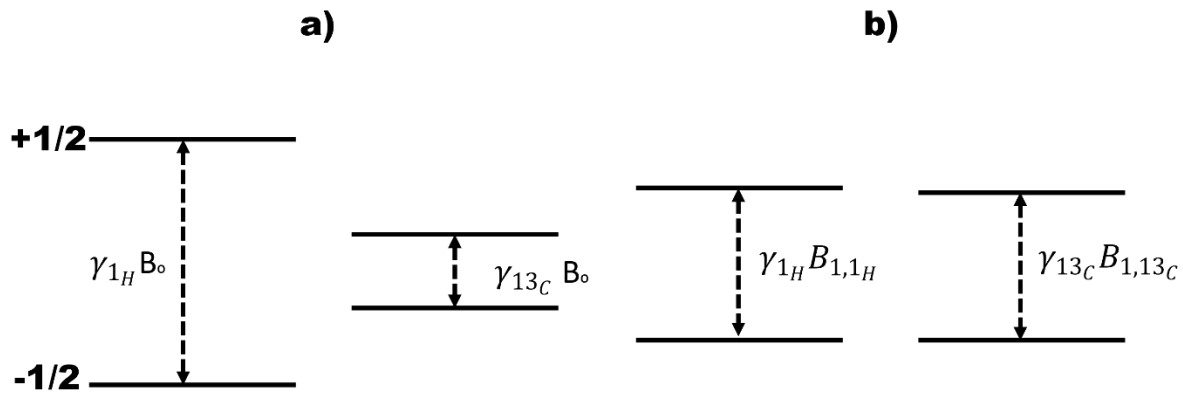


**Figure 1.6** Energy levels of $^{1}$H (abundant nuclei) and $^{13}$C (rare nuclei) spin in the laboratory frame (a) and in the rotating frame of reference (b). In b, the Hartmann Hahn matching condition is fulfilled.

Cross polarization is a technique that is used to enhance the signal intensity of less abundant nuclei.[52] This technique was introduced first by Hartmann and Hahn in 1962 for static conditions.[53] The most common nuclear species that is used for transferring polarization is $^{1}$H due to its high natural abundance (99.9%) and high gyromagnetic ratio (γ), which are the two basic requirements for high sensitivity in NMR spectra. Even though the protons are extremely sensitive nuclei, $^{1}$H spectra are generally poorly resolved due to the dense proton network with strong homonuclear couplings and little dispersion of proton signals. Hence, $^{13}$C is frequently selected as the preferred nucleus due to its extensive spectral width of 200 ppm. Since $^{13}$C has a lower gyromagnetic ratio i.e.,1/4 of γH), low abundance, and long spin-lattice relaxation ($T_1$), suitable labeling strategies and cross-polarization are required for obtaining good signal-to-noise.

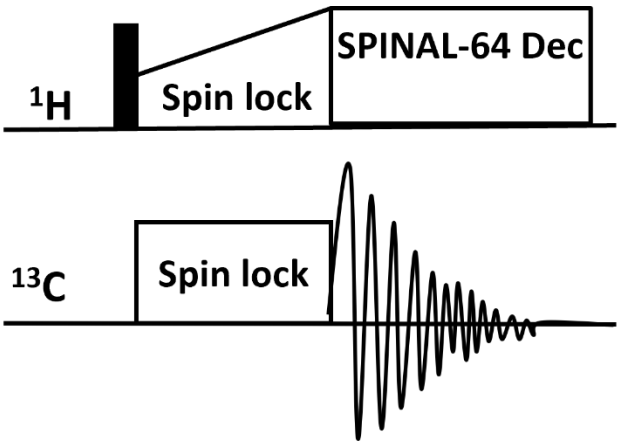


**Figure 1.7** represents the pulse sequence for cross polarization.

In the CP method, an initial 90° pulse establishes transverse magnetization in the rotating frame after which a contact pulse is applied on resonance with the $^{1}H$ and it creates a transverse field $B_{1,1_H}$ that is static in the rotating frame and is called a spin lock field. Simultaneously, a contact pulse on $^{13}C$ is applied, which gives rise to a spin lock field $B_{1,13_C}$. For the polarization transfer to occur the nutation frequencies of both the nuclei must be identical and match the Hartmann Hann matching condition according to[41]

$\gamma_{1_H} B_{1,1_H} = \gamma_{13_C} B_{1,13_C}$ .

(11)

The signal obtained after polarization transfer is enhanced by decoupling protons from carbon.

The Hartmann-Hahn match condition is modified when it is being used under MAS, and it is given by

$\gamma_{1_H} B_{1,1_H} - \gamma_{13_C} B_{1,13_C} = \pm n\omega_r$

(12)

where *n* is an integer.[41,54]

**Insensitive Nuclei Enhanced by Polarization Transfer (INEPT)**

INEPT is a technique that is being employed to enhance the magnetization of the nuclear isotopes with a low gyromagnetic ratio.[55] Unlike CP, the INEPT sequence works by transferring magnetization through a bond and not through space. Through bond transfer is usually seen in solution NMR, whereas *J* coupling has minor contributions to the spin Hamiltonian of solids. Yet this technique has been proven to be powerful for transferring polarization where there are significant dynamics in the biological solids and the dipolar couplings get averaged to zero.

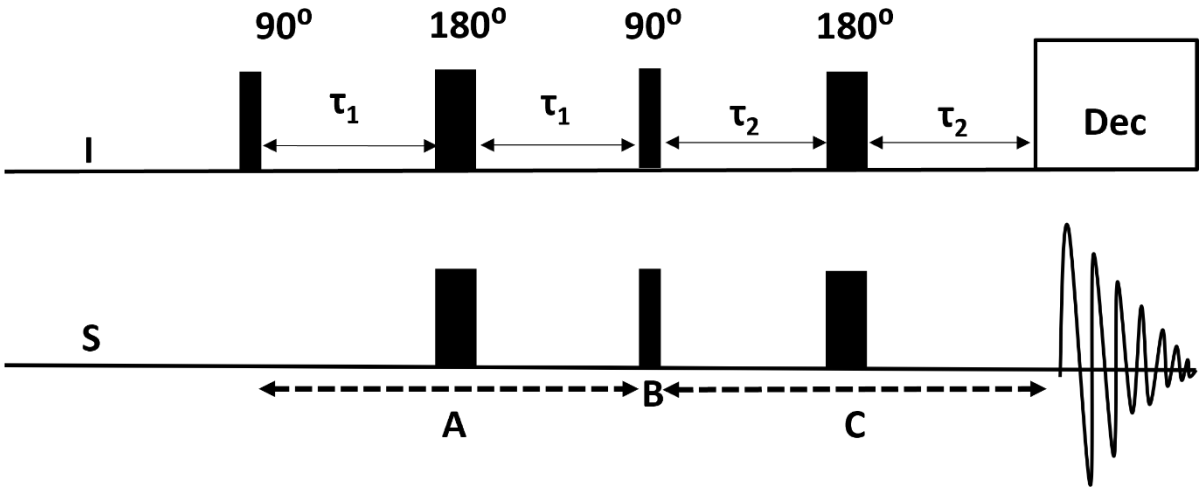


**Figure 1.8** represents the pulse sequence for INEPT.

During A, an antiphase state is generated for the I spin, *i.e.* $^{1}$H. During B, the antiphase state is transferred to S, *i.e.* $^{13}$C. During C, the antiphase state evolves back to an in-phase state that is observed on the S channel. The pulse sequence begins with a 90º pulse on the spin I to create transverse magnetization. A spin echo is applied to both spins to refocus the chemical shifts while the coupling continues to evolve for the whole period of $2\tau_1$. During B, the two 90º pulses on both channels transfer the antiphase state from the I spin to the S spin. During C, again we apply a spin echo during which the couplings continue to evolve, and the antiphase state is converted to an in-phase state. The detailed explanation of the INEPT transfer steps can be found in[42,47,56]. The optimum values for both delays are $\tau_{1,2} = 1/4J_{IS}$.

## 1.8 Advanced Solid-State NMR techniques used in this present study.

The broadband homonuclear recoupling techniques used in this study are PDSD, RFDR, CHHC and INEPT-TOBSY, while hCH, scalar hCH, and REDOR have been employed as heteronuclear recoupling techniques.

**Homonuclear dipolar correlation experiments used in this study:**

**Proton Driven Spin Diffusion (PDSD)**

PDSD is one of the oldest recoupling techniques. It is being employed to study the transfer of magnetization from $^{13}$C-$^{13}$C directly through space, and is mediated by interaction with the protons.[57,58]

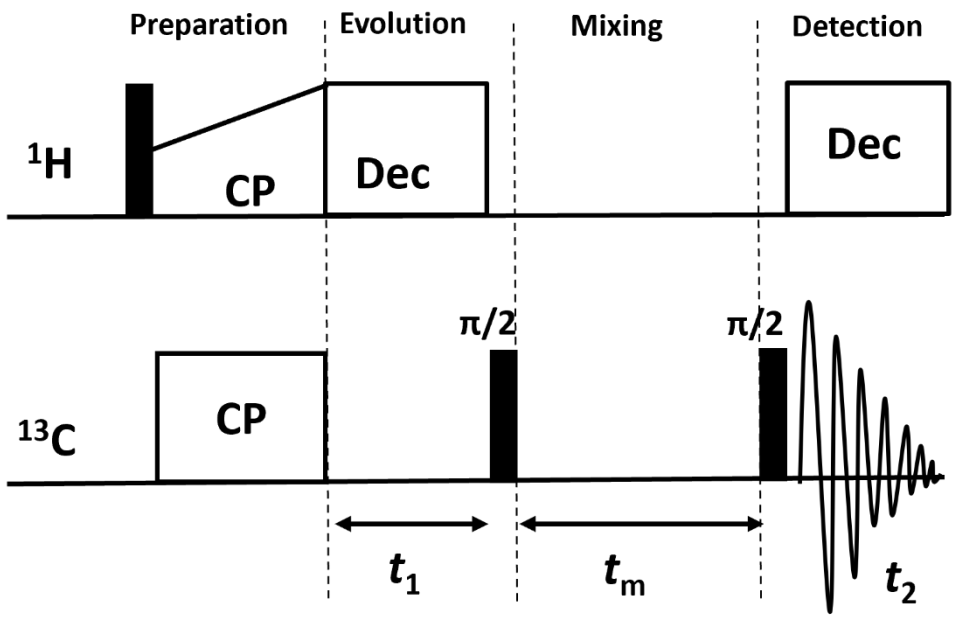


**Figure 1.9** represents the pulse sequence for proton driven spin diffusion.

There are four steps in the pulse sequence, namely preparation, evolution, mixing and detection. CPMAS is used during the preparation step to enhance the $^{13}$C magnetization, which results in a spin-locked $^{13}$C magnetization in the xy plane. During evolution, the dilute $^{13}$C spins are subjected to a Zeeman interaction under the influence of a $^{13}$C chemical shift Hamiltonian and under strong proton decoupling. The 90º pulse after the evolution time maps the chemical shift information on $^{13}$C magnetization in the *z* direction. During the mixing period, $^{13}$C spins communicate with each other. There is an exchange of polarization, and protons aid in this mixing process. The last step is a detection step where a 90º pulse at the end of the mixing period is used to reestablish observable $^{13}$C magnetization. This technique does not use any radiofrequency field during mixing, which makes it a preferred choice of experiment for biological assemblies or proteins. It is also a versatile experiment if the sample is fully labeled and there is dipolar truncation, this experiment works best.[59,60]

**Radio Frequency Driven Recoupling (RFDR)**

This is a homonuclear dipolar recoupling experiment that was used in the present study to assign the $^{13}$C chemical shifts.

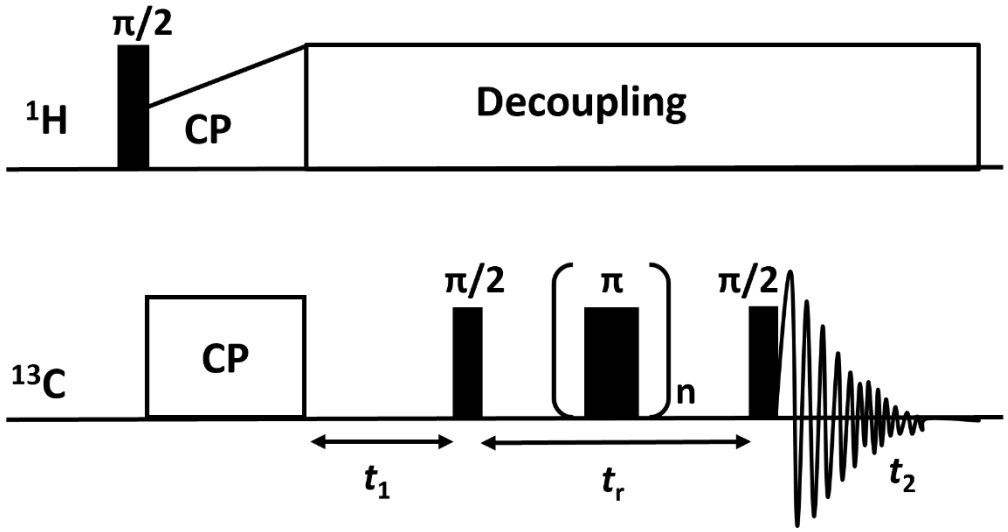


**Figure 1.10** represents a pulse sequence for RFDR. The rotor period is denoted by a symbol $\tau_r$, and n represents the train of rotor synchronized π pulses.

The pulse sequence for RFDR begins with the application of a 90º pulse on the $^{1}H$, followed by polarization transfer to the $^{13}C$ through cross polarization. After the CP step, a train of rotor-synchronised π pulses are applied on the carbon channel while simultaneously decoupling the protons. This reintroduces the homonuclear $^{13}C$ dipolar couplings that are averaged due to MAS.[61]

**CHHC/CP$^3$ Experiment**

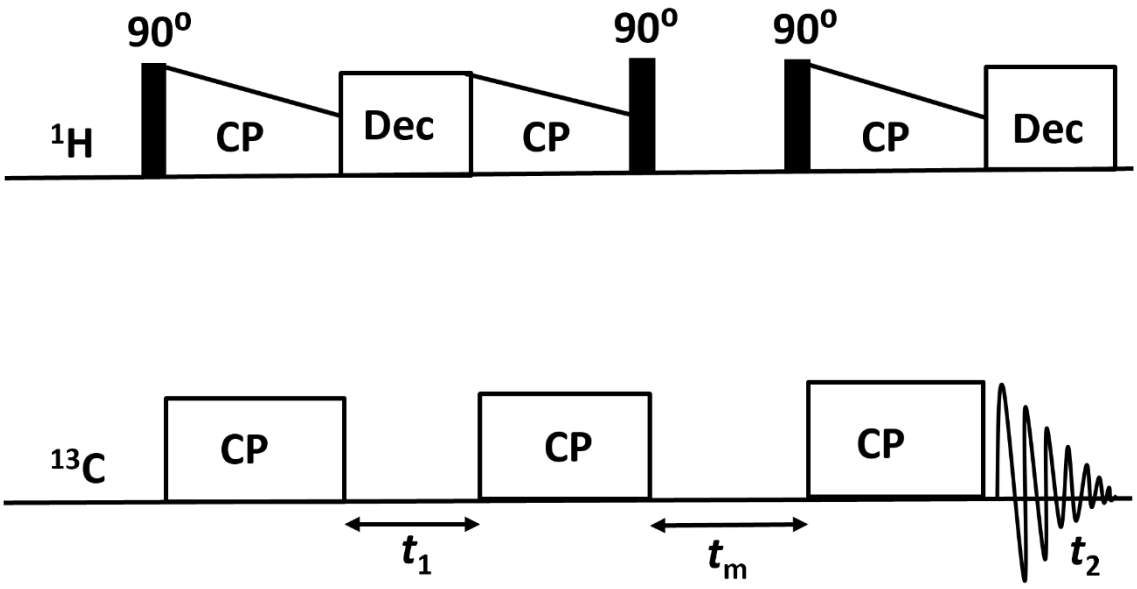


**Figure 1.11** represents the pulse sequence for CHHC.

The CHHC pulse sequence is used to probe the distance constraints in the present study. The pulse sequence begins with the first CP, where the proton magnetization is transferred to the carbons, followed by decoupling of the protons and evolution of $^{13}C$ chemical shifts during $t_1$. During the second CP, the $^{13}C$ magnetization is transferred back to the protons and the proton magnetization is stored along the magnetic field $B_0$ by the application of a 90º pulse. During the $t_m$ period, the proton magnetization is distributed by proton spin diffusion. Short mixing times of 0.1 to 1 ms time range should be used during the mixing period. Then, a second 90º pulse is applied to rotate the proton magnetization back to the XY plane, followed by a final CP for high-resolution $^{13}C$ detection.[62] This method is employed for probing the proton distance constraints by making use of a dense proton network for the spin diffusion. This enables the detection of the polarization transfer properties of $^{1}H$ spins with rare spin evolution and detection periods in solid-state NMR.[62–64]

**INEPT-TOBSY (TOtal through Bond correlation SpectroscopY)**

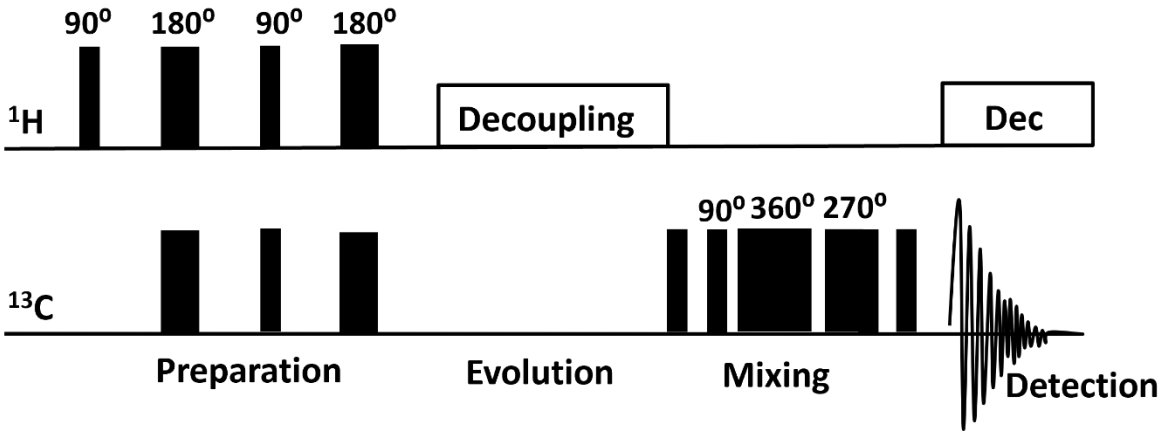


**Figure 1.12** represents the pulse sequence for INEPT-TOBSY.

Total through bond correlation spectroscopy is used to exploit the J-coupling interactions of the spin system. INEPT is used as a prefix because it is used for enhancing the magnetization during the preparation step, instead of CP, which is commonly used. During TOBSY, the homo and heteronuclear dipolar interactions as well as the chemical shifts, must be suppressed during the mixing period so that the dominant interaction in the Hamiltonian is the isotropic J coupling. To suppress these interactions use of fast spinning and the application of rotor synchronized π pulses can be used at high spinning speeds, and at low spinning speeds, efficient proton decoupling methods like Lee-Goldberg are mostly used.[65,66]

**Heteronuclear correlation experiments used in this present study:**

The **Dipolar hCH/ CP-HSQC** technique was used to assign the protons. This is a proton-detected experiment. The advantage of proton detection lies in its high natural abundance and high gyromagnetic ratio. However, the same condition poses a problem due to the dense proton network and strong homonuclear dipolar couplings. Thanks to the high field and small rotors, the resolution and sensitivity are significantly improved.[67–70]

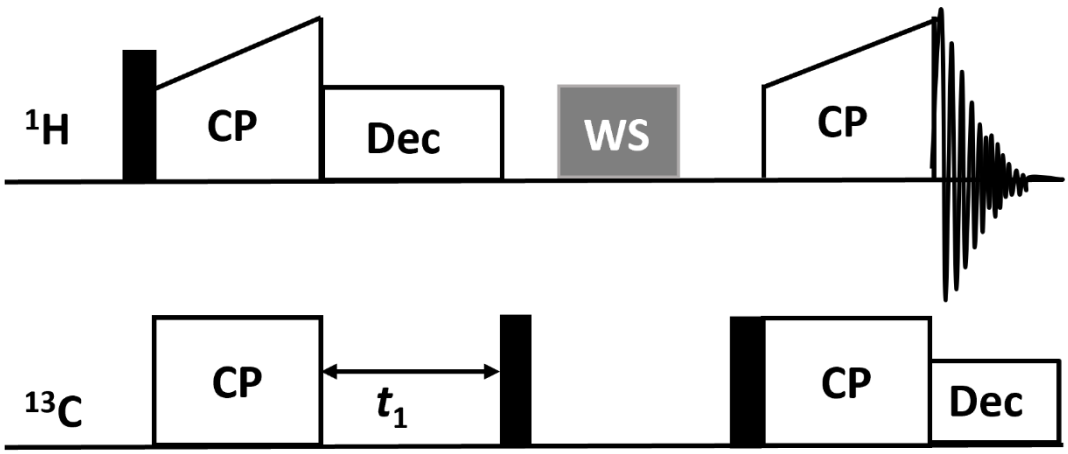


**Figure 1.13** represents the pulse sequence for dipolar-hCH.

Here, the pulse sequence begins with the cross polarization from proton to carbons during the first CP after which the evolution of $^{13}C$ chemical shifts takes place and the simultaneous decoupling of protons. A 90º pulse on the carbon channel projects the $^{13}C$ magnetization onto the z axis followed by a certain delay for dephasing any remaining transverse $^{1}H$ magnetization. The grey box indicates a water suppression block to remove any residual water signal. The final CP block transfers the magnetization back to protons where it is being detected.[68,71]

INEPT-hCH uses an INEPT block for magnetization transfer and it is used to assign mobile residues. The pulse sequence follows the above sequence, where the CP blocks are replaced by INEPT.

**Rotational Echo DOuble Resonance (REDOR)**

To study the C-H dipolar coupling strength, the distances between C-H were determined by using $^{13}C\{^{1}H\}$ REDOR.[72–78] REDOR works by reintroducing the dipolar couplings that are averaged due to MAS by application of π pulses every half a rotor period and dipolar dephasing is observed which attenuates the signal intensity of the observed signal.[79] The datasets are collected by two consecutive experiments with and without π pulses which gives S and $S_0$ data sets from dipolar dephasing and natural dephasing respectively, $S_0$ accounts for

the dephasing due to relaxation. The intensity difference between these two allows us to extract the dipolar coupling strength by comparing it with computer simulations.[49,50]

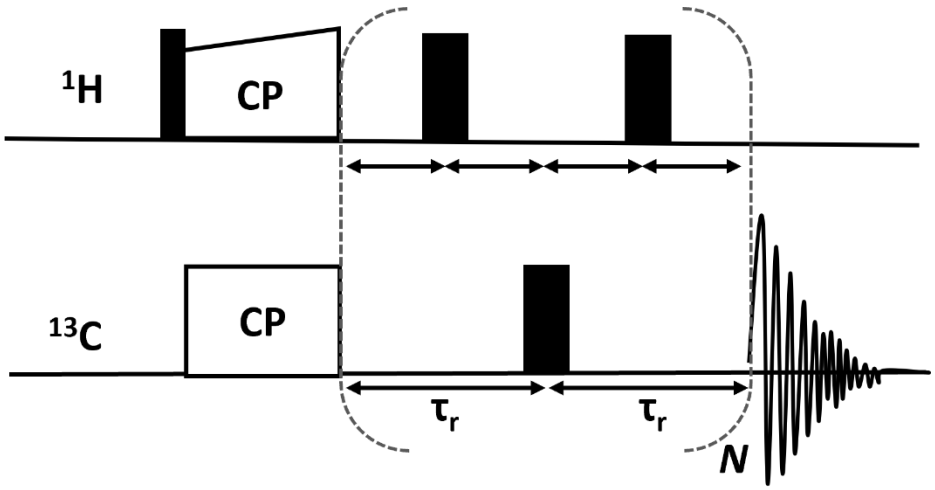


**Figure 1.14** represents the pulse sequence for REDOR. The rotor period is denoted by a symbol $\tau_r$, and N represents the number of times the $\pi$ pulses are repeated.

## Objectives and Scope of the Thesis

The overarching aim of this thesis is to deepen the understanding of the molecular mechanisms underlying light harvesting in green sulfur bacteria. Specifically, the work focuses on elucidating the structural organization and conformational dynamics of chlorosome antenna complexes, which represent the largest and most efficient light-harvesting systems found in nature. Solid-state NMR spectroscopy is employed as the primary characterization technique over the last decade, particularly those inaccessible to solution-state NMR or X-ray crystallography providing atomistic insights into both the static arrangement and the dynamic flexibility of bacteriochlorophyll aggregates within chlorosomes.[80–85]

The scope of the thesis extends beyond structural description to include a comparative investigation of chlorosomes from wild-type *Chlorobaculum tepidum* and genetically modified strains such as *bchQ* and *bchR*. This allows for an assessment of how pigment composition and side-chain modifications influence the architecture, dynamics, and functionality of the antenna system. Complementary approaches, including cryo-electron microscopy and optical spectroscopy, are also incorporated to provide a multidimensional perspective that integrates molecular, supramolecular, and functional levels of organization. Together, these studies aim to establish a comprehensive framework for linking structural and

dynamic features of chlorosomes to their exceptional efficiency in capturing and transferring solar energy, thereby offering insights of relevance not only to biology but also to the design of bio-inspired light-harvesting systems.Additionally, the use of dynamic spectral editing techniques has also paved the way for studying the site-specific dynamics of BChl pigments.[43,50,86–89]

**Chapter 2** provides an understanding of the structure of the *bchQ* mutant of *Cba. tepidum* and its comparison to WT using distance constraints obtained from solid-state NMR in combination with cryo-EM and optical spectroscopy. In addition to the structure, it also gives a preliminary understanding of dynamics in comparison to the WT.

**Chapter 3** explains the conformational dynamics of the *bchQ* mutant of *Cba. tepidum* in detail by making use of solid-state NMR techniques. To address the site-specific dynamics of chlorosomes, we utilized the MAS NMR $^{1}$H-$^{13}$C polarization transfer dynamic spectral editing (DYSE) approach. To explore the rotational motion of BChl *c* within the stack, we employ a direct measurement of the dipolar coupling between a C-H pair located at a meso-position of the macrocycle using Rotational Echo Double Resonance (REDOR). The 5C-H meso-position is selected because it is clearly distinguished from other carbon positions, making it well-suited for REDOR measurements. By using REDOR, which provides direct access to the strength of dipolar coupling, we can investigate this coupling and compare our results to the expected values under conditions of complete rigidity.

**Chapter 4** reveals the dynamics of chlorosomes of WT of *Cba. tepidum* using DYSE, PDSD and relaxation measurements. It also shows the plastic crystallinity of chlorosomes of WT using REDOR to address the macrocycle dynamics. A similar approach to that of Chapter 3 is employed to study the site-specific dynamics and librational motion.

**Chapter 5** presents preliminary data on the chlorosomes from the *bchR* mutant, which exhibits variations in the methylation patterns of the 12$^{1}$ BChl side chain. To examine structural and dynamic changes, I utilized magic angle spinning nuclear magnetic resonance (MAS NMR).

**Chapter 6** demonstrates how solid-state NMR can be used to resolve the microscopic organization of chlorosomes in *Cba. tepidum* within their native cellular environment.It also explains the dynamics of chlorosomes inside a native cell using DYSE techniques.

Finally, a general discussion and prospectives related to chlorosomes of *Cba. tepidum* are provided in **Chapter 7**

# References


(1) Purchase, R. L.; de Groot, H. J. M. Biosolar Cells: Global Artificial Photosynthesis Needs Responsive Matrices with Quantum Coherent Kinetic Control for High Yield. *Interface Focus.* **2015**, *5* (3), 20150014. https://doi.org/10.1098/rsfs.2015.0014.

(2) de Lorenzo, V.; Prather, K. L.; Chen, G.; O'Day, E.; von Kameke, C.; Oyarzún, D. A.; Hosta-Rigau, L.; Alsafar, H.; Cao, C.; Ji, W.; Okano, H.; Roberts, R. J.; Ronaghi, M.; Yeung, K.; Zhang, F.; Lee, S. Y. The Power of Synthetic Biology for Bioproduction, Remediation and Pollution Control. *EMBO Rep* **2018**, *19* (4), e45658. https://doi.org/10.15252/embr.201745658.

(3) Gust, D.; Moore, T. A.; Moore, A. L. Solar Fuels via Artificial Photosynthesis. *Acc. Chem. Res.* **2009**, *42* (12), 1890–1898. https://doi.org/10.1021/ar900209b.

(4) McConnell, I.; Li, G.; Brudvig, G. W. Energy Conversion in Natural and Artificial Photosynthesis. *Chemistry & Biology* **2010**, *17* (5), 434–447. https://doi.org/10.1016/j.chembiol.2010.05.005.

(5) Frischmann, P. D.; Mahata, K.; Würthner, F. Powering the Future of Molecular Artificial Photosynthesis with Light-Harvesting Metallosupramolecular Dye Assemblies. *Chem. Soc. Rev.* **2013**, *42* (4), 1847–1870. https://doi.org/10.1039/C2CS35223K.

(6) Croce, R.; van Amerongen, H. Natural Strategies for Photosynthetic Light Harvesting. *Nat Chem Biol* **2014**, *10* (7), 492–501. https://doi.org/10.1038/nchembio.1555.

(7) Croce, R.; Takahashi, Y. Chapter 15 - Photosynthesis: Light Harvesting. In *The Chlamydomonas Sourcebook (Third Edition)*; Grossman, A. R., Wollman, F.-A., Eds.; Academic Press: London, 2023; pp 509–524. https://doi.org/10.1016/B978-0-12-821430-5.00026-2.

(8) Mirkovic, T.; Ostroumov, E. E.; Anna, J. M.; van Grondelle, R.; Govindjee; Scholes, G. D. Light Absorption and Energy Transfer in the Antenna Complexes of Photosynthetic Organisms. *Chem. Rev.* **2017**, *117* (2), 249–293. https://doi.org/10.1021/acs.chemrev.6b00002.

(9) Frontmatter. In *Molecular Mechanisms of Photosynthesis*; John Wiley & Sons, Ltd, 2002; pp i–vii. https://doi.org/10.1002/9780470758472.fmatter.

(10) Kaiser, E.; Morales, A.; Harbinson, J.; Kromdijk, J.; Heuveink, E.; Marcelis, L. F. M. Dynamic Photosynthesis in Different Environmental Conditions. *Journal of Experimental Botany* **2014**. https://doi.org/10.1093/jxb/eru406.

(11) Wolf, Y. I.; Katsnelson, M. I.; Koonin, E. V. Physical Foundations of Biological Complexity. *Proceedings of the National Academy of Sciences* **2018**, *115* (37), E8678–E8687. https://doi.org/10.1073/pnas.1807890115.

(12) Matsubara, S.; Tamiaki, H. Supramolecular Chlorophyll Aggregates Inspired from Specific Light-Harvesting Antenna "Chlorosome": Static Nanostructure, Dynamic Construction Process, and Versatile Application. *Journal of Photochemistry and Photobiology C: Photochemistry Reviews* **2020**, *45*, 100385. https://doi.org/10.1016/j.jphotochemrev.2020.100385.

(13) Ganapathy, S.; Sengupta, S.; Wawrzyniak, P. K.; Huber, V.; Buda, F.; Baumeister, U.; Würthner, F.; de Groot, H. J. M. Zinc Chlorins for Artificial Light-Harvesting Self-Assemble into Antiparallel Stacks Forming a Microcrystalline Solid-State Material. *PNAS* **2009**, *106* (28), 11472–11477. https://doi.org/10.1073/pnas.0811872106.

(14) Löhner, A.; Kunsel, T.; Röhr, M. I. S.; Jansen, T. L. C.; Sengupta, S.; Würthner, F.; Knoester, J.; Köhler, J. Spectral and Structural Variations of Biomimetic Light-Harvesting Nanotubes. *J. Phys. Chem. Lett.* **2019**, *10* (11), 2715–2724. https://doi.org/10.1021/acs.jpclett.9b00303.

(15) Huber, V.; Katterle, M.; Lysetska, M.; Würthner, F. Reversible Self-Organization of Semisynthetic Zinc Chlorins into Well-Defined Rod Antennae. *Angewandte Chemie International Edition* **2005**, *44* (20), 3147–3151. https://doi.org/10.1002/anie.200462762.

(16) Huber, V.; Lysetska, M.; Würthner, F. Self-Assembled Single- and Double-Stack π-Aggregates of Chlorophyll Derivatives on Highly Ordered Pyrolytic Graphite. *Small* **2007**, *3* (6), 1007–1014. https://doi.org/10.1002/smll.200600497.

(17) Holzwarth, A. R.; Griebenow, K.; Schaffner, K. Chlorosomes, Photosynthetic Antennae with Novel Self-Organized Pigment Structures. *Journal of Photochemistry and Photobiology A: Chemistry* **1992**, *65* (1), 61–71. https://doi.org/10.1016/1010-6030(92)85032-P.

(18) Kundu, S.; Patra, A. Nanoscale Strategies for Light Harvesting. *Chem. Rev.* **2017**, *117* (2), 712–757. https://doi.org/10.1021/acs.chemrev.6b00036.

(19) Idi, A.; Md Nor, M. H.; Abdul Wahab, M. F.; Ibrahim, Z. Photosynthetic Bacteria: An Eco-Friendly and Cheap Tool for Bioremediation. *Rev Environ Sci Biotechnol* **2015**, *14* (2), 271–285. https://doi.org/10.1007/s11157-014-9355-1.

(20) Bryant, D. A.; Frigaard, N.-U. Prokaryotic Photosynthesis and Phototrophy Illuminated. *Trends in Microbiology* **2006**, *14* (11), 488–496. https://doi.org/10.1016/j.tim.2006.09.001.

(21) George, D. M.; Vincent, A. S.; Mackey, H. R. An Overview of Anoxygenic Phototrophic Bacteria and Their Applications in Environmental Biotechnology for Sustainable Resource Recovery. *Biotechnol Rep (Amst)* **2020**, *28*, e00563. https://doi.org/10.1016/j.btre.2020.e00563.

(22) Beatty, J. T.; Overmann, J.; Lince, M. T.; Manske, A. K.; Lang, A. S.; Blankenship, R. E.; Van Dover, C. L.; Martinson, T. A.; Plumley, F. G. An Obligately Photosynthetic Bacterial Anaerobe from a Deep-Sea Hydrothermal Vent. *Proceedings of the National Academy of Sciences* **2005**, *102* (26), 9306–9310. https://doi.org/10.1073/pnas.0503674102.

(23) *Candidatus Chloracidobacterium thermophilum: An Aerobic Phototrophic Acidobacterium*. https://doi.org/10.1126/science.1143236.

(24) Oostergetel, G. T.; van Amerongen, H.; Boekema, E. J. The Chlorosome: A Prototype for Efficient Light Harvesting in Photosynthesis. *Photosynth Res* **2010**, *104* (2–3), 245–255. https://doi.org/10.1007/s11120-010-9533-0.

(25) Overmann, J.; Cypionka, H.; Pfennig, N. An Extremely Low-Light Adapted Phototrophic Sulfur Bacterium from the Black Sea. *Limnology and Oceanography* **1992**, *37* (1), 150–155. https://doi.org/10.4319/lo.1992.37.1.0150.

(26) *Physiology and Phylogeny of Green Sulfur Bacteria Forming a Monospecific Phototrophic Assemblage at a Depth of 100 Meters in the Black Sea*. https://doi.org/10.1128/AEM.71.12.8049-8060.2005.

(27) Borrego, C. M.; Garcia-Gil, L. J. Rearrangement of Light Harvesting Bacteriochlorophyll Homologues as a Response of Green Sulfur Bacteria to Low Light Intensities. *Photosynth Res* **1995**, *45* (1), 21–30. https://doi.org/10.1007/BF00032232.

(28) Borrego, C. M.; Gerola, P. D.; Miller, M.; Cox, R. P. Light Intensity Effects on Pigment Composition and Organisation in the Green Sulfur Bacterium Chlorobium Tepidum. *Photosynthesis Research* **1999**, *59* (2), 159–166. https://doi.org/10.1023/A:1006161302838.

(29) Marschall, E.; Jogler, M.; Henßge, U.; Overmann, J. Large-Scale Distribution and Activity Patterns of an Extremely Low-Light-Adapted Population of Green Sulfur Bacteria in the Black Sea. *Environmental Microbiology* **2010**, *12* (5), 1348–1362. https://doi.org/10.1111/j.1462-2920.2010.02178.x.

(30) Orf, G. S.; Blankenship, R. E. Chlorosome Antenna Complexes from Green Photosynthetic Bacteria. *Photosynth Res* **2013**, 17.

(31) Frigaard, N.-U.; Bryant, D. A. Chlorosomes: Antenna Organelles in Photosynthetic Green Bacteria. In *Complex Intracellular Structures in Prokaryotes*; Shively, J. M., Ed.; Microbiology Monographs; Springer Berlin Heidelberg: Berlin, Heidelberg, 2006; Vol. 2, pp 79–114. https://doi.org/10.1007/7171_021.

(32) Bryant, D. A.; Canniffe, D. P. How Nature Designs Light-Harvesting Antenna Systems: Design Principles and Functional Realization in Chlorophototrophic Prokaryotes. *J. Phys. B: At. Mol. Opt. Phys.* **2018**, *51* (3), 033001. https://doi.org/10.1088/1361-6455/aa9c3c.

(33) Andrew Staehelin, L.; Golecki, J. R.; Drews, G. Supramolecular Organization of Chlorosomes (Chlorobium Vesicles) and of Their Membrane Attachment Sites in Chlorobium Limicola. *Biochimica et Biophysica Acta (BBA) - Bioenergetics* **1980**, *589* (1), 30–45. https://doi.org/10.1016/0005-2728(80)90130-9.

(34) Nielsen, J. T.; Kulminskaya, N. V.; Bjerring, M.; Linnanto, J. M.; Rätsep, M.; Pedersen, M. Ø.; Lambrev, P. H.; Dorogi, M.; Garab, G.; Thomsen, K.; Jegerschöld, C.; Frigaard, N.-U.; Lindahl, M.; Nielsen, N. C. In Situ High-Resolution Structure of the Baseplate Antenna Complex in Chlorobaculum Tepidum. *Nat Commun* **2016**, *7* (1), 12454. https://doi.org/10.1038/ncomms12454.

(35) Vassilieva, E. V.; Stirewalt, V. L.; Jakobs, C. U.; Frigaard, N.-U.; Inoue-Sakamoto, K.; Baker, M. A.; Sotak, A.; Bryant, D. A. Subcellular Localization of Chlorosome Proteins in Chlorobium Tepidum and Characterization of Three New Chlorosome Proteins: CsmF, CsmH, and CsmX. *Biochemistry* **2002**, *41* (13), 4358–4370. https://doi.org/10.1021/bi012051u.

(36) Frigaard, N.-U.; Bryant, D. A. Seeing Green Bacteria in a New Light: Genomics-Enabled Studies of the Photosynthetic Apparatus in Green Sulfur Bacteria and Filamentous Anoxygenic Phototrophic Bacteria. *Arch Microbiol* **2004**, *182* (4), 265–276. https://doi.org/10.1007/s00203-004-0718-9.

(37) Chen, J.-H.; Wu, H.; Xu, C.; Liu, X.-C.; Huang, Z.; Chang, S.; Wang, W.; Han, G.; Kuang, T.; Shen, J.-R.; Zhang, X. Architecture of the Photosynthetic Complex from a Green Sulfur Bacterium. *Science* **2020**, *370* (6519), eabb6350. https://doi.org/10.1126/science.abb6350.

(38) Camara-Artigas, A.; Blankenship, R. E.; Allen, J. P. The Structure of the FMO Protein from Chlorobium Tepidum at 2.2 A Resolution. *Photosynth Res* **2003**, *75* (1), 49–55. https://doi.org/10.1023/A:1022406703110.

(39) Büttner, M.; Xie, D. L.; Nelson, H.; Pinther, W.; Hauska, G.; Nelson, N. Photosynthetic Reaction Center Genes in Green Sulfur Bacteria and in Photosystem 1 Are Related. *Proc Natl Acad Sci U S A* **1992**, *89* (17), 8135–8139.

(40) Abragam, A. *The Principles of Nuclear Magnetism*; Clarendon Press, 1983.

(41) Duer, M. J. *Introduction to Solid-State NMR Spectroscopy*; Blackwell Publishing: Oxford [etc, 2004.

(42) Levitt, M. H. *Spin Dynamics : Basics of Nuclear Magnetic Resonance*; Wiley: Chichester [etc, 2001.

(43) Matlahov, I.; van der Wel, P. C. A. Hidden Motions and Motion-Induced Invisibility: Dynamics-Based Spectral Editing in Solid-State NMR. *Methods* **2018**, *148*, 123–135. https://doi.org/10.1016/j.ymeth.2018.04.015.

(44) Andrew, E. R.; Bradbury, A.; Eades, R. G. Removal of Dipolar Broadening of Nuclear Magnetic Resonance Spectra of Solids by Specimen Rotation. *Nature* **1959**, *183* (4678), 1802–1803. https://doi.org/10.1038/1831802a0.

(45) Lowe, I. J. Free Induction Decays of Rotating Solids. *Phys. Rev. Lett.* **1959**, *2* (7), 285–287. https://doi.org/10.1103/PhysRevLett.2.285.

(46) Schaefer, J.; Stejskal, E. O. Carbon-13 Nuclear Magnetic Resonance of Polymers Spinning at the Magic Angle. *J. Am. Chem. Soc.* **1976**, *98* (4), 1031–1032. https://doi.org/10.1021/ja00420a036.

(47) Morris, G. A.; Freeman, R. Enhancement of Nuclear Magnetic Resonance Signals by Polarization Transfer. *J. Am. Chem. Soc.* **1979**, *101* (3), 760–762. https://doi.org/10.1021/ja00497a058.

(48) Gustavsson, S.; Alves, L.; Lindman, B.; Topgaard, D. Polarization Transfer Solid-State NMR: A New Method for Studying Cellulose Dissolution. *RSC Adv.* **2014**, *4* (60), 31836–31839. https://doi.org/10.1039/C4RA04415K.

(49) Azadi Chegeni, F.; Perin, G.; Sai Sankar Gupta, K. B.; Simionato, D.; Morosinotto, T.; Pandit, A. Protein and Lipid Dynamics in Photosynthetic Thylakoid Membranes Investigated by In-Situ Solid-State NMR. *Biochimica et Biophysica Acta (BBA) - Bioenergetics* **2016**, *1857* (12), 1849–1859. https://doi.org/10.1016/j.bbabio.2016.09.004.

(50) van der Wel, P. C. A. New Applications of Solid-State NMR in Structural Biology. *Emerging Topics in Life Sciences* **2018**, *2* (1), 57–67. https://doi.org/10.1042/ETLS20170088.

(51) Pandit, A. Structural Dynamics of Light Harvesting Proteins, Photosynthetic Membranes, and Cells Observed by Spectral Editing Solid-State NMR. *The Journal of Chemical Physics* **2022**, *157* (2), 025101. https://doi.org/10.1063/5.0094446.

(52) Pines, A.; Gibby, M. G.; Waugh, J. S. Proton-enhanced NMR of Dilute Spins in Solids. *The Journal of Chemical Physics* **1973**, *59* (2), 569–590. https://doi.org/10.1063/1.1680061.

(53) Hartmann, S. R.; Hahn, E. L. Nuclear Double Resonance in the Rotating Frame. *Phys. Rev.* **1962**, *128* (5), 2042–2053. https://doi.org/10.1103/PhysRev.128.2042.

(54) Stejskal, E. O.; Schaefer, J.; Waugh, J. S. Magic-Angle Spinning and Polarization Transfer in Proton-Enhanced NMR. *Journal of Magnetic Resonance (1969)* **1977**, *28* (1), 105–112. https://doi.org/10.1016/0022-2364(77)90260-8.

(55) Fyfe, C. A.; Wong-Moon, K. C.; Huang, Y.; Grondey, H. INEPT Experiments in Solid-State NMR. *J. Am. Chem. Soc.* **1995**, *117* (41), 10397–10398. https://doi.org/10.1021/ja00146a031.

(56) Keeler, James. *Understanding NMR Spectroscopy*; Wiley: Chichester, 2005.

(57) Szeverenyi, N. M.; Sullivan, M. J.; Maciel, G. E. Observation of Spin Exchange by Two-Dimensional Fourier Transform 13C Cross Polarization-Magic-Angle Spinning. *Journal of Magnetic Resonance (1969)* **1982**, *47* (3), 462–475. https://doi.org/10.1016/0022-2364(82)90213-X.

(58) Suter, D.; Ernst, R. R. Spectral Spin Diffusion in the Presence of an Extraneous Dipolar Reservoir. *Phys. Rev. B* **1982**, *25* (9), 6038–6041. https://doi.org/10.1103/PhysRevB.25.6038.

(59) Grommek, A.; Meier, B. H.; Ernst, M. Distance Information from Proton-Driven Spin Diffusion under MAS. *Chemical Physics Letters* **2006**, *427* (4), 404–409. https://doi.org/10.1016/j.cplett.2006.07.005.

(60) Veshtort, M.; Griffin, R. G. Proton-Driven Spin Diffusion in Rotating Solids via Reversible and Irreversible Quantum Dynamics. *The Journal of Chemical Physics* **2011**, *135* (13), 134509. https://doi.org/10.1063/1.3635374.

(61) Bennett, A. E.; Griffin, R. G.; Ok, J. H.; Vega, S. Chemical Shift Correlation Spectroscopy in Rotating Solids: Radio Frequency-driven Dipolar Recoupling and

Longitudinal Exchange. *The Journal of Chemical Physics* **1992**, *96* (11), 8624–8627. https://doi.org/10.1063/1.462267.

(62) De Boer, I.; Bosman, L.; Raap, J.; Oschkinat, H.; De Groot, H. J. M. 2D13C–13C MAS NMR Correlation Spectroscopy with Mixing by True 1H Spin Diffusion Reveals Long-Range Intermolecular Distance Restraints in Ultra High Magnetic Field. *Journal of Magnetic Resonance* **2002**, *157* (2), 286–291. https://doi.org/10.1006/jmre.2002.2588.

(63) Lange, A.; Seidel, K.; Verdier, L.; Luca, S.; Baldus, M. Analysis of Proton−Proton Transfer Dynamics in Rotating Solids and Their Use for 3D Structure Determination. *J. Am. Chem. Soc.* **2003**, *125* (41), 12640–12648. https://doi.org/10.1021/ja034555g.

(64) Lange, A.; Luca, S.; Baldus, M. Structural Constraints from Proton-Mediated Rare-Spin Correlation Spectroscopy in Rotating Solids. *J. Am. Chem. Soc.* **2002**, *124* (33), 9704–9705. https://doi.org/10.1021/ja026691b.

(65) Baldus, M.; Meier, B. H. Total Correlation Spectroscopy in the Solid State. The Use of Scalar Couplings to Determine the Through-Bond Connectivity. *Journal of Magnetic Resonance, Series A* **1996**, *121* (1), 65–69. https://doi.org/10.1006/jmra.1996.0137.

(66) Hardy, E. H.; Verel, R.; Meier, B. H. Fast MAS Total Through-Bond Correlation Spectroscopy. *Journal of Magnetic Resonance* **2001**, *148* (2), 459–464. https://doi.org/10.1006/jmre.2000.2258.

(67) Andreas, L. B.; Le Marchand, T.; Jaudzems, K.; Pintacuda, G. High-Resolution Proton-Detected NMR of Proteins at Very Fast MAS. *J Magn Reson* **2015**, *253*, 36–49. https://doi.org/10.1016/j.jmr.2015.01.003.

(68) Barbet-Massin, E.; Pell, A. J.; Retel, J. S.; Andreas, L. B.; Jaudzems, K.; Franks, W. T.; Nieuwkoop, A. J.; Hiller, M.; Higman, V.; Guerry, P.; Bertarello, A.; Knight, M. J.; Felletti, M.; Le Marchand, T.; Kotelovica, S.; Akopjana, I.; Tars, K.; Stoppini, M.; Bellotti, V.; Bolognesi, M.; Ricagno, S.; Chou, J. J.; Griffin, R. G.; Oschkinat, H.; Lesage, A.; Emsley, L.; Herrmann, T.; Pintacuda, G. Rapid Proton-Detected NMR Assignment for Proteins with Fast Magic Angle Spinning. *J. Am. Chem. Soc.* **2014**, *136* (35), 12489–12497. https://doi.org/10.1021/ja507382j.

(69) Le Marchand, T.; Schubeis, T.; Bonaccorsi, M.; Paluch, P.; Lalli, D.; Pell, A. J.; Andreas, L. B.; Jaudzems, K.; Stanek, J.; Pintacuda, G. 1H-Detected Biomolecular NMR under Fast Magic-Angle Spinning. *Chem. Rev.* **2022**, *122* (10), 9943–10018. https://doi.org/10.1021/acs.chemrev.1c00918.

(70) Callon, M.; Malär, A. A.; Pfister, S.; Římal, V.; Weber, M. E.; Wiegand, T.; Zehnder, J.; Chávez, M.; Cadalbert, R.; Deb, R.; Däpp, A.; Fogeron, M.-L.; Hunkeler, A.; Lecoq, L.;

Torosyan, A.; Zyla, D.; Glockshuber, R.; Jonas, S.; Nassal, M.; Ernst, M.; Böckmann, A.; Meier, B. H. Biomolecular Solid-State NMR Spectroscopy at 1200 MHz: The Gain in Resolution. *J Biomol NMR* **2021**, *75* (6–7), 255–272. https://doi.org/10.1007/s10858-021-00373-x.

(71) Paulson, E. K.; Morcombe, C. R.; Gaponenko, V.; Dancheck, B.; Byrd, R. A.; Zilm, K. W. Sensitive High Resolution Inverse Detection NMR Spectroscopy of Proteins in the Solid State. *J. Am. Chem. Soc.* **2003**, *125* (51), 15831–15836. https://doi.org/10.1021/ja037315+.

(72) Cui, J.; Olmsted, D. L.; Mehta, A. K.; Asta, M.; Hayes, S. E. NMR Crystallography: Evaluation of Hydrogen Positions in Hydromagnesite by 13C1H REDOR Solid-State NMR and Density Functional Theory Calculation of Chemical Shielding Tensors. *Angewandte Chemie International Edition* **2019**, *58* (13), 4210–4216. https://doi.org/10.1002/anie.201813306.

(73) Ishii, Y.; Wickramasinghe, N. P.; Chimon, S. A New Approach in 1D and 2D 13C High-Resolution Solid-State NMR Spectroscopy of Paramagnetic Organometallic Complexes by Very Fast Magic-Angle Spinning. *J. Am. Chem. Soc.* **2003**, *125* (12), 3438–3439. https://doi.org/10.1021/ja0291742.

(74) Celinski, V. R.; Weber, J.; Schmedt Auf Der Günne, J. C-REDOR Curves of Extended Spin Systems. *Solid State Nuclear Magnetic Resonance* **2013**, *49–50*, 12–22. https://doi.org/10.1016/j.ssnmr.2012.10.001.

(75) Wickramasinghe, N. P.; Shaibat, M. A.; Jones, C. R.; Casabianca, L. B.; De Dios, A. C.; Harwood, J. S.; Ishii, Y. Progress in C13 and H1 Solid-State Nuclear Magnetic Resonance for Paramagnetic Systems under Very Fast Magic Angle Spinning. *The Journal of Chemical Physics* **2008**, *128* (5), 052210. https://doi.org/10.1063/1.2833574.

(76) Dasgupta, R.; Gupta, K. B. S. S.; Elam, D.; Ubbink, M.; de Groot, H. J. M. Dipolar Dephasing for Structure Determination in a Paramagnetic Environment. *Solid State Nuclear Magnetic Resonance* **2021**, *113*, 101728. https://doi.org/10.1016/j.ssnmr.2021.101728.

(77) Sinha, N.; Hong, M. X–1H Rotational-Echo Double-Resonance NMR for Torsion Angle Determination of Peptides. *Chemical Physics Letters* **2003**, *380* (5–6), 742–748. https://doi.org/10.1016/j.cplett.2003.09.088.

(78) Hou, G.; Byeon, I.-J. L.; Ahn, J.; Gronenborn, A. M.; Polenova, T. 1H–13C/1H–15N Heteronuclear Dipolar Recoupling by R-Symmetry Sequences Under Fast Magic Angle

Spinning for Dynamics Analysis of Biological and Organic Solids. *J. Am. Chem. Soc.* **2011**, *133* (46), 18646–18655. https://doi.org/10.1021/ja203771a.

(79) Grage, S. L.; Watts, A. Applications of REDOR for Distance Measurements in Biological Solids. In *Annual Reports on NMR Spectroscopy*; Webb, G. A., Ed.; Academic Press, 2006; Vol. 60, pp 191–228. https://doi.org/10.1016/S0066-4103(06)60005-7.

(80) Lange, A.; Becker, S.; Seidel, K.; Giller, K.; Pongs, O.; Baldus, M. A Concept for Rapid Protein-Structure Determination by Solid-State NMR Spectroscopy. *Angewandte Chemie International Edition* **2005**, *44* (14), 2089–2092. https://doi.org/10.1002/anie.200462516.

(81) Castellani, F.; van Rossum, B.; Diehl, A.; Schubert, M.; Rehbein, K.; Oschkinat, H. Structure of a Protein Determined by Solid-State Magic-Angle-Spinning NMR Spectroscopy. *Nature* **2002**, *420* (6911), 99–102. https://doi.org/10.1038/nature01070.

(82) Ganapathy, S.; Oostergetel, G. T.; Wawrzyniak, P. K.; Reus, M.; Gomez Maqueo Chew, A.; Buda, F.; Boekema, E. J.; Bryant, D. A.; Holzwarth, A. R.; de Groot, H. J. M. Alternating Syn-Anti Bacteriochlorophylls Form Concentric Helical Nanotubes in Chlorosomes. *Proceedings of the National Academy of Sciences* **2009**, *106* (21), 8525–8530. https://doi.org/10.1073/pnas.0903534106.

(83) Ganapathy, S.; Oostergetel, G. T.; Reus, M.; Tsukatani, Y.; Gomez Maqueo Chew, A.; Buda, F.; Bryant, D. A.; Holzwarth, A. R.; de Groot, H. J. M. Structural Variability in Wild-Type and *BchQ BchR* Mutant Chlorosomes of the Green Sulfur Bacterium *Chlorobaculum Tepidum*. *Biochemistry* **2012**, *51* (22), 4488–4498. https://doi.org/10.1021/bi201817x.

(84) Zech, S. G.; Wand, A. J.; McDermott, A. E. Protein Structure Determination by High-Resolution Solid-State NMR Spectroscopy: Application to Microcrystalline Ubiquitin. *J. Am. Chem. Soc.* **2005**, *127* (24), 8618–8626. https://doi.org/10.1021/ja0503128.

(85) Lecoq, L.; Fogeron, M.-L.; Meier, B. H.; Nassal, M.; Böckmann, A. Solid-State NMR for Studying the Structure and Dynamics of Viral Assemblies. *Viruses* **2020**, *12* (10), 1069. https://doi.org/10.3390/v12101069.

(86) Lin, H.-K.; Boatz, J. C.; Krabbendam, I. E.; Kodali, R.; Hou, Z.; Wetzel, R.; Dolga, A. M.; Poirier, M. A.; van der Wel, P. C. A. Fibril Polymorphism Affects Immobilized Non-Amyloid Flanking Domains of Huntingtin Exon1 Rather than Its Polyglutamine Core. *Nat Commun* **2017**, *8* (1), 15462. https://doi.org/10.1038/ncomms15462.

(87) Azadi-Chegeni, F.; Ward, M. E.; Perin, G.; Simionato, D.; Morosinotto, T.; Baldus, M.; Pandit, A. Conformational Dynamics of Light-Harvesting Complex II in a Native Membrane Environment. *Biophysical Journal* **2021**, *120* (2), 270–283. https://doi.org/10.1016/j.bpj.2020.11.2265.

(88) Azadi-Chegeni, F.; Schiphorst, C.; Pandit, A. In Vivo NMR as a Tool for Probing Molecular Structure and Dynamics in Intact Chlamydomonas Reinhardtii Cells. *Photosynth Res* **2018**, *135* (1–3), 227–237. https://doi.org/10.1007/s11120-017-0412-9.

(89) Nami, F.; Tian, L.; Huber, M.; Croce, R.; Pandit, A. Lipid and Protein Dynamics of Stacked and Cation-Depletion Induced Unstacked Thylakoid Membranes. *BBA Advances* **2021**, *1*, 100015. https://doi.org/10.1016/j.bbadva.2021.100015.